

Department of Atmospheric Sciences, National Central University
Chair Professor Lectures supported by the MOST, Taiwan

Dynamical Mountain Meteorology

Dr. Yuh-Lang Lin, ylin@cat.edu; <http://mesolab.ncat.edu>
North Carolina A&T State University
(Ref.: *Mesoscale Dynamics*, Y.-L. Lin, Cambridge, 2007)

Chapter 10 Three-Dimensional Flow over Isolated Mountains

(Based on “Flow over Three-Dimensional Mountains”, Sec. 5.4 of *Mesoscale Dynamics* (Lin 2007))
(Classical equation editor: $c_p \neq f(k)$)

10.1 Three-Dimensional Flow over Isolated Mountains

(Flow over three-dimensional mountains)

Although the two-dimensional mountain wave theories discussed in previous sections helped explain some important flow phenomena generated by infinitely long ridges, such as upward propagating mountains waves, lee waves, wave overturning and breaking, and severe downslope winds, in reality most of the mountains are of three-dimensional, complex form.

The basic dynamics of flow over complex terrain can be understood by considering flow over an idealized, three-dimensional, isolated mountain.

In this section, we will discuss a linear theory of a stratified flow past an isolated mountain, as well as the generation of lee vortices in a nonlinear flow over an isolated mountain.

10.1.1 Linear theory

In the following, the two-dimensional, linear mountain wave theory developed in Section 5.2.1 is extended to three-dimensional flow over an isolated mountain.

Consider a steady state, small-amplitude, adiabatic, inviscid, nonrotating, stratified, Boussinesq fluid flow with uniform basic velocity (U) and Brunt-Vaisala frequency (N) over a three-dimensional topography $h(x, y)$.

The governing linear equations can be derived from (5.1.1)-(5.1.4),

$$U \frac{\partial u'}{\partial x} + \frac{1}{\rho_o} \frac{\partial p'}{\partial x} = 0, \quad (5.4.1)$$

$$U \frac{\partial v'}{\partial x} + \frac{1}{\rho_o} \frac{\partial p'}{\partial y} = 0, \quad (5.4.2)$$

$$U \frac{\partial w'}{\partial x} - g \frac{\theta'}{\theta_o} + \frac{1}{\rho_o} \frac{\partial p'}{\partial z} = 0, \quad (5.4.3)$$

$$\frac{\partial u'}{\partial x} + \frac{\partial v'}{\partial y} + \frac{\partial w'}{\partial z} = 0, \quad (5.4.4)$$

$$U \frac{\partial \theta'}{\partial x} + \frac{N^2 \theta_o}{g} w' = 0. \quad (5.4.5)$$

Using (5.1.19), the above equations can be combined into a single equation of η ,

$$\nabla^2 \eta_{xx} + \frac{N^2}{U^2} \nabla_H^2 \eta = 0. \quad (5.4.6)$$

Equation (5.4.6) can be solved by taking the double Fourier transform in x and y to obtain

$$\hat{\eta}_{zz} + m^2 \hat{\eta} = 0, \quad (5.4.7)$$

where

$$m^2 = K^2 (N^2 / k^2 U^2 - 1), \quad (5.4.8)$$

and $K = \sqrt{k^2 + l^2}$ is the horizontal wavenumber.

The double Fourier transform pair is defined as

$$\hat{\eta}(k, l, z) = \frac{1}{4\pi^2} \int_{-\infty}^{\infty} \int_{-\infty}^{\infty} \eta(x, y, z) e^{-i(kx+ly)} dx dy, \quad (5.4.9a)$$

$$\eta(x, y, z) = \int_{-\infty}^{\infty} \int_{-\infty}^{\infty} \hat{\eta}(k, l, z) e^{i(kx+ly)} dk dl. \quad (5.4.9b)$$

The solution to (5.4.7) in the Fourier space can be found

$$\hat{\eta}(k, l, z) = \hat{\eta}(k, l, 0) e^{im(k,l)z}. \quad (5.4.10)$$

Similar to the two-dimensional mountain wave theory, as discussed in section 5.2, there exist two flow regimes:

- (I) $N^2 / k^2 U^2 > 1$
- (II) $N^2 / k^2 U^2 < 1$

For **upward propagating waves (regime I)**, the sign of m must be the same as the sign of k , in order to satisfy the upper radiation condition.

On the other hand, for **evanescent waves (regime II)**, the positive root of (5.4.8) must be chosen, i.e.

$$\hat{\eta}(k, l, z) = \hat{\eta}(k, l, 0) e^{-m_i(k, l)z}, \quad (5.4.11)$$

Where m_i is defined as $K\sqrt{1 - N^2 / k^2 U^2}$.

The linear lower boundary condition is

$$\eta(x, y, z = 0) = h(x, y), \quad (5.4.12)$$

which can be transformed into the Fourier space,

$$\hat{\eta}(k, l, 0) = \hat{h}(k, l). \quad (5.4.13)$$

From the definition of inverse Fourier transform and (5.4.13), we have

$$\eta(x, y, z) = \int_{-\infty}^{\infty} \int_{-\infty}^{\infty} \hat{h}(k, l) e^{im(k, l)z} e^{i(kx+ly)} dk dl. \quad (5.4.14)$$

Now let us consider a three-dimensional (circular) bell-shaped mountain

$$h(x, y) = \frac{h}{(r^2 / a^2 + 1)^{3/2}}; \quad r = \sqrt{x^2 + y^2}, \quad (5.4.15)$$

Where h and a are the mountain height and horizontal scale, respectively. The Fourier transform of (5.4.15) is,

$$\hat{h}(k, l) = \frac{ha^2}{2\pi} e^{-aK}. \quad (5.4.16)$$

The problem may be further simplified by using the hydrostatic approximation, i.e. neglecting the first term of (5.4.3). Note that under the hydrostatic approximation, we require that $Na/U \gg 1$.

The solution, (5.4.14), may be reduced to a single integration by converting it into cylindrical coordinates, and asymptotic solutions for the flow aloft and the flow near the ground may thus be obtained (Smith 1980).

Substituting (5.4.16) into (5.4.14) and nondimensionalizing it according to

$$(\tilde{x}, \tilde{y}) = (x/a, y/a), (\tilde{z}, \tilde{\eta}) = (Nz/U, N\eta/U), (\tilde{k}, \tilde{l}, \tilde{K}) = (ka, la, Ka), \quad (5.4.17)$$

yields

$$\tilde{\eta}(\tilde{x}, \tilde{y}, \tilde{z}) = \frac{1}{F} \int_{-\infty}^{\infty} \int_{-\infty}^{\infty} e^{-\tilde{K}} e^{i\tilde{m}\tilde{z}} e^{i(\tilde{k}\tilde{x} + \tilde{l}\tilde{y})} d\tilde{k} d\tilde{l} , \quad (5.4.18)$$

where F is the Froude number, as defined earlier.

As discussed earlier, the linear theory holds for a large Froude number flow.

On the other hand, for a small Froude number flow, nonlinear effects become more important and cannot be ignored. This will be discussed in the next subsection.

Equation (5.4.18) or (5.4.14) can also be solved numerically by applying a two-dimensional numerical FFT algorithm.

Figure 5.17 shows an example of a linear, hydrostatic flow passing over a bell-shaped mountain with a Froude number of 100.

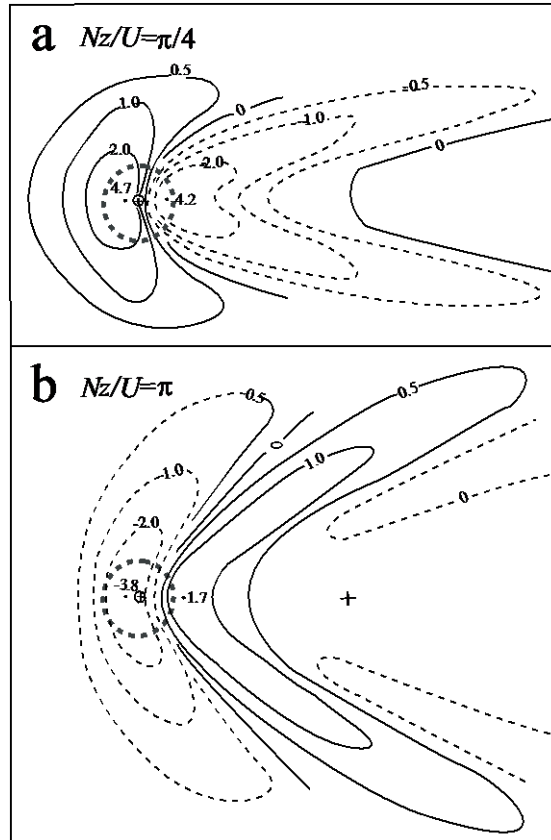


Fig. 5.17: Three-dimensional, linear, hydrostatic stratified flow over a bell-shaped mountain (5.4.15) with $F = U/Nh = 100$. The basic flow is from left to right. Displayed are the nondimensional vertical displacement at $\tilde{z} = Nz/U = :$ (a) $\pi/4$ and (b) π . U-shaped disturbances are associated with the upward propagating wave energy. Solid and dashed curves represent positive and negative values of vertical displacement. The cross marks the position of the mountain peak. The bold, dashed circle is the topographic contour at $r = a$, where r is the distance (radius) from the center of the mountain. These wave patterns are computed by evaluating (5.4.18) numerically using a two-dimensional FFT. (Adapted after Smith 1980)

- Near the surface, the pattern of vertical displacement resembles the surface topography, (5.4.15), as required by the lower boundary condition.
- Slightly aloft from the surface at $\tilde{z} = \pi/4$ (Fig. 5.17a), a region of downward displacement forms a U-shaped

disturbance over the lee slopes of the mountain and extends some distance downstream.

- At a level further aloft, such as $\tilde{z} = \pi$ (Fig. 5.17b), the region of downward displacement widens, moves upstream, and is replaced by a U-shaped pattern of upward displacement.
 - The general upstream shift of downward and upward displacement is caused by the upstream phase tilt of upward propagating hydrostatic waves.
 - At greater heights, the zone of disturbance continues to broaden, the disturbance directly in the lee of the mountain disappears, and the patterns of upward and downward displacement become more wavelike, due to wave dispersion.
- The U-shaped patterns of vertical displacements are explained by a group velocity argument (Smith 1980). The dispersion relation for internal gravity waves in a stagnant Boussinesq fluid may be reduced from (3.6.10)

$$\omega = \frac{\pm NK}{\sqrt{k^2 + l^2 + m^2}}. \quad (5.4.19)$$

With the hydrostatic approximation the above equation becomes

$$\omega = \pm \frac{NK}{m}. \quad (5.4.20)$$

As discussed in Chapter 4, the energy propagation can be described by the group velocity components, which are

$$c_{gx} = \frac{\partial \omega}{\partial k} = \pm \frac{Nk}{mK}; \quad c_{gy} = \frac{\partial \omega}{\partial l} = \pm \frac{Nl}{mK}; \quad c_{gz} = \frac{\partial \omega}{\partial m} = \mp \frac{NK}{m^2} \quad (5.4.21)$$

For steady-state waves on a basic flow, replacing ω by the intrinsic frequency Uk in (5.4.20) leads to

$$m = \frac{\pm NK}{Uk}. \quad (5.4.22)$$

Adding U to c_{gx} , the components of the group velocity in a frame fixed with the Earth become

$$c_{gmx} = \frac{Ul^2}{K^2}; \quad c_{gmy} = \frac{-Ukl}{K^2}; \quad c_{gmz} = \frac{U^2k^2}{NK}. \quad (5.4.23)$$

- In the coordinates fixed with the mountain or Earth, wave energy propagates from the energy source, i.e. the mountain, along straight lines with slopes

$$\frac{x}{z} = \frac{c_{gmx}}{c_{gmz}}; \quad \frac{y}{z} = \frac{c_{gmy}}{c_{gmz}}; \quad \frac{y}{x} = \frac{c_{gmy}}{c_{gmx}}. \quad (5.4.24)$$

The slope on the horizontal plane y/x may be evaluated from (5.4.23) and (5.4.24),

$$\frac{y}{x} = -\frac{k}{l}, \quad (5.4.25)$$

which is the geometric condition that the phase lines passing through the point (x, y) are radial lines from the origin.

Using (5.4.23)-(5.4.24) again gives

$$y^2 = \frac{Nxz}{UK}. \quad (5.4.26)$$

Since the mountain is the source of forcing, the horizontal wavenumber may be approximated by the mountain scale, i.e. $K \approx 1/a$, which yields

$$y^2 = \left(\frac{Nax}{U} \right) z. \quad (5.4.27)$$

Thus, the energy concentrates in a parabola or a U-shaped pattern at a certain height, as shown in Fig. 5.17.

- In the above theory, the basic flow speed and Brunt-Vaisala frequency are assumed to be constant with height. In the real atmosphere, they normally vary with height.

As in the two-dimensional mountain wave problem, a rapid decrease of the Scorer parameter with height leads to the formation of *trapped lee waves*.

The formation of three-dimensional trapped lee waves is similar to that of *Kelvin ship waves* over the water surface.

Figure 5.18 shows an example of the cloud streets associated with three-dimensional trapped lee waves produced by airflow past a mountainous island.

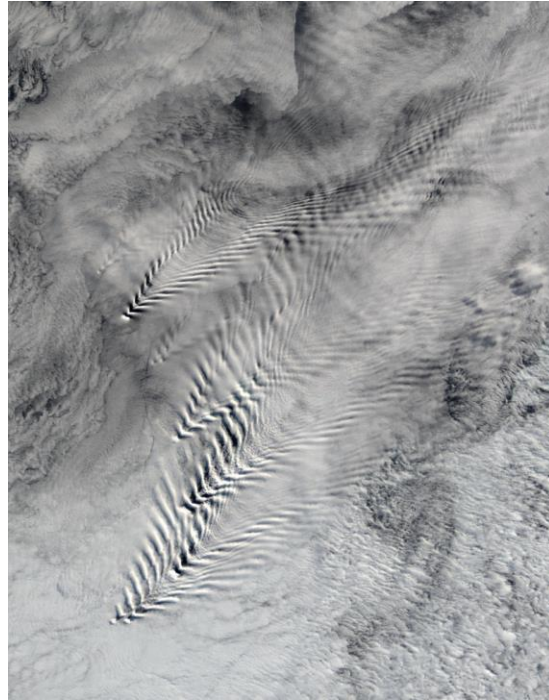


Fig. 5.18: Satellite imagery of three-dimensional trapped lee waves induced by the South Sandwich Islands in southern Atlantic Ocean on September 18, 2003. The wave pattern is similar to that of the ship waves sketched in Fig. 5.19. (From Visible Earth, NASA)

The wave pattern is generally contained within a wedge with the apex at the mountain. The three-dimensional trapped lee waves are composed by *transverse waves* and *diverging waves*, as depicted in Fig. 5.19.

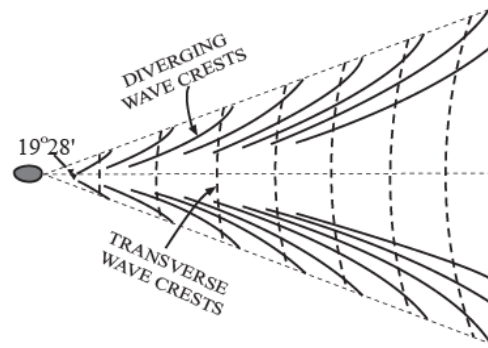


Fig. 5.19: Schematic of transverse (bold-dashed) and diverging (solid) phase lines for a deep water ship wave. (Adapted after Sharman and Wurtele 1983)

- The transverse waves lie approximately perpendicular to the flow direction, and are formed by waves attempting to propagate against the basic flow but that have been advected to the lee.

The formation mechanism of transverse waves is the same as that of the two-dimensional trapped lee waves.

- Unlike the transverse waves, the diverging waves attempt to propagate laterally away from the mountain and have been advected to the lee.

Also, the diverging waves have crests that meet the incoming flow at a rather shallow angle.

- Both of the transverse and diverging waves are mathematically associated with a stationary phase point, and the significant disturbance is confined within a wedge angle of about $19^{\circ}28'$ with the x -axis.

○

(10/29/14)

10.1.2 Generation of lee vortices

The above linear theory of three-dimensional, stratified flow over mountains is valid only for high Froude number flow due to the limitations of the small-amplitude (linear) assumption.

When the Froude number decreases, the perturbations generated by the mountain become larger and the flow becomes more nonlinear.

Due to mathematical intractability, many observed phenomena associated with nonlinear flow over mountains, such as flow recirculation, stagnation points, flow splitting, and lee vortices, have been carried out in tank experiments and by nonlinear numerical simulations.

a. Boundary layer separation

The flow pattern produced by laboratory tank experiments for three-dimensional, stratified flow with relatively large Froude numbers (e.g. $F > 2$) past a bell-shaped mountain is similar to that predicted by linear theory as described in subsection 5.4.1. Flow patterns are dramatically different for flow with smaller Froude numbers.

Figure 5.20 shows a stratified flow with $F=0.4$ past an isolated mountain in a tank experiment.

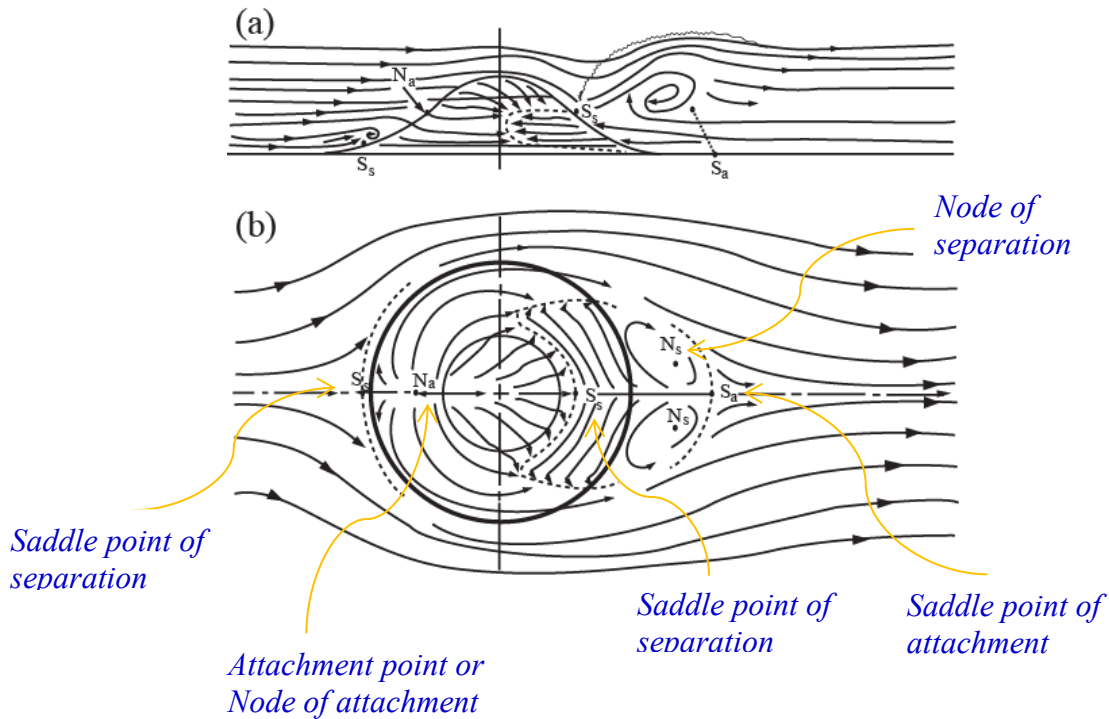


Fig. 5.20: (a) Side view of the mean surface shear stress pattern and streamlines on the center plane of symmetry for a three-dimensional, stratified, viscous flow with $F = U / Nh = 0.4$ past an obstacle with circular contours (e.g., bold solid curve in (b)). In the figure, N and S denote nodes and saddle points, respectively, and subscripts a and s denote attachment and separation, respectively. (b) As (a) but for a plane view of the pattern of surface stress. (Adapted after Hunt and Snyder 1980)

The most eye-catching phenomenon is a pair of counter-rotating vortices formed in the lee of the obstacle. The formation of this pair of lee vortices is attributed to the *boundary layer separation mechanism* (Batchelor 1967; Hunt and Snyder 1980), as briefly summarized in the following.

- When the Reynolds number (Re) is sufficiently high (where $Re = UL/\nu$, U is the velocity scale, L the length scale and ν the kinematic viscosity; show the derivation of Re), the boundary-layer flow develops a region of flow reversal near the surface due to an opposing pressure gradient in the direction of flow.

- The reversed flow meets the incoming flow and forms a **stagnation point** at which the streamline breaks away from the surface of the obstacle. This process is known as *boundary layer separation*.
 - Mathematically, the streamline of boundary layer separation is a line whose points are singular points of the solutions of the equations of motion in the boundary layer.
- For three-dimensional, nonlinear, stratified viscous flow past a symmetric mountain, **boundary layer separation first occurs on the center vertical plane before the mountain peak is reached**.

During the process, several singular points can form.

- Over the upslope on the center plane, an *attachment point (node of attachment)* N_a forms,

which forces part of the flow to recirculate back upstream along the upslope, where it meets the incoming flow, and forms another stagnation point (*saddle point of separation*) S_s (Fig. 5.20a).

- Downstream of the obstacle on the center vertical plane, flow separates and forms a third stagnation point(s) (*saddle points of attachment*) S_a .

- The separated flow recirculates on this vertical plane, meets with the downslope flow and forms another *saddle point of separation* (S_s) over the lee slope.
- On the surface (Fig. 5.20b), the recirculated flow from N_a forces the incoming flow to split (i.e. *flow splitting*) at s_s and part of the split flow recirculates and forms a pair of stationary lee vortices centered at the *nodes of separation* (N_s).
- If the Froude number is decreased further, this flow pattern persists, but N_a moves closer to the mountain peak and the lee vortices expand further downstream.
- Although an unrealistically large mountain slope of $O(1)$, compared to that in the real world is often used in laboratory experiments, the simulated flow features are very similar to those observed in the real atmosphere.

b. Generation of lee vortices in an inviscid fluid

- Using a nonlinear numerical model with free-slip lower boundary condition, a pair of counter-rotating vortices was found to form on the lee of an isolated mountain when a **low-Froude number** (e.g., $F = 0.66$, Fig. 5.21a), **three-dimensional, stratified, uniform flow passes over the mountain** (Smolarkiewicz and Rotunno 1989).

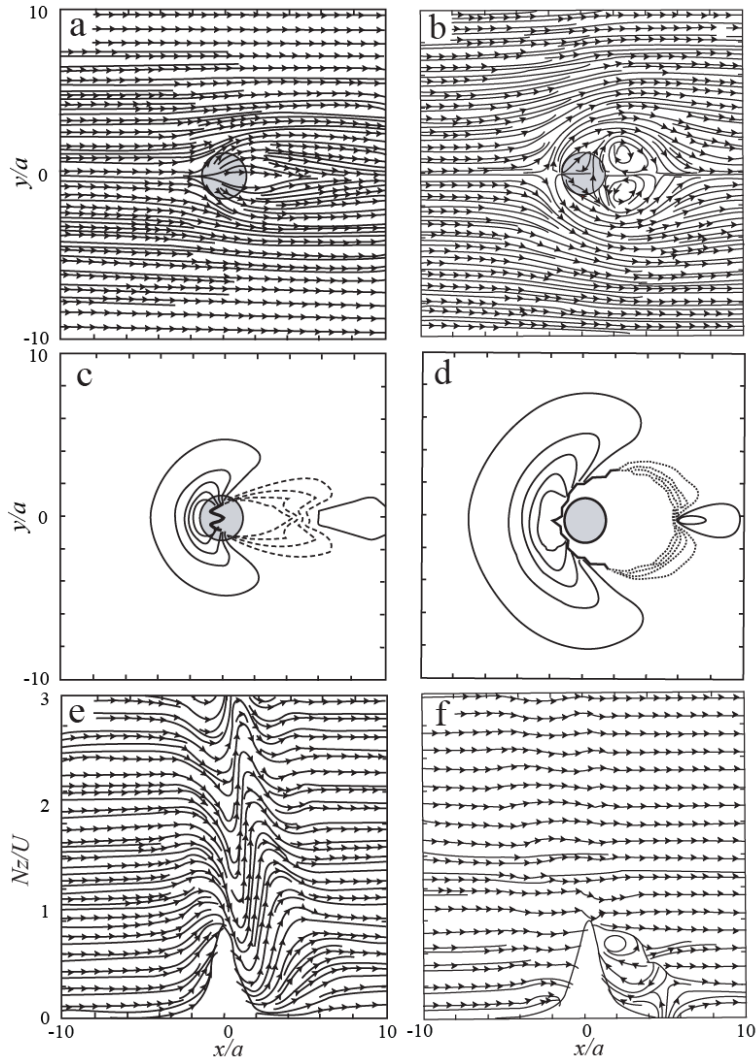


Fig. 5.21: Three-dimensional, stratified, uniform flow with no surface friction over a bell-shaped mountain simulated by a nonlinear numerical model. Surface streamlines, vertical displacements at $Nz/U = \pi/4$, and streamlines in the vertical plane $y/a = 0$ after $Ut/a = 9$ are shown in (a), (c), and (e), respectively, for the case with $F = 0.66$. The same flow fields but for $F = 0.22$ are shown in the right panels ((b),(d) and (f)). The simulated flow fields have reached quasi-steady state. The flow and orographic parameters are: $U = 10\text{ms}^{-1}$ or 3.3ms^{-1} , $N = 0.01\text{ s}^{-1}$, $h = 1.5\text{ km}$, and $a = 10\text{ km}$, which give $F = 0.66$ or 0.22 , respectively. The bell-shaped mountain is prescribed by (5.4.15). (Adapted after Smolarkiewicz and Rotunno 1989)

The simulated results agree fairly well with laboratory tank experiments as shown in Fig. 5.20.

The free-slip lower boundary condition implies no explicit surface friction is included in the model atmosphere.

Although linear theory breaks down, at least locally, the vertical displacement field (Fig. 5.21c) still resembles the U-shaped pattern found in the linear theory described in subsection 5.4.1 (Fig. 5.17).

A large-amplitude mountain wave develops over the mountain peak (Fig. 5.21e). The trough of the vertically propagating gravity waves in Fig. 5.21e shifts upstream and becomes narrower, indicating a tendency toward collapse of the isentropic surfaces on the lee slopes of the mountain, which is also in agreement with the linear theory. Since the air parcels are able to flow almost directly across the mountain, this flow regime is characterized as the *flow-over regime*.

When the Froude number is reduced to approximately below 0.5, such as $F = 0.22$ (Fig. 5.21b), the following flow characteristics are observed:

- A pair of counter-rotating vortices forms on the lee side and a saddle point of separation and a node of attachment are produced on the upstream side of the mountain, strikingly similar to the results obtained in laboratory experiments (Fig. 5.20b).
- The region of downward displacement is enlarged (Fig. 5.21d).
- The gravity wave response is drastically reduced, as much of the airflow is diverted around the flanks of the

mountain and the disturbance appears to be much more horizontal (Fig. 5.21f).

- Below the mountain top, there is a recirculating flow associated with the **lee vortices**. This flow regime is characterized as the *flow-around regime*.

➤ Based on the nondimensional mountain height (Nh/U , also called inverse Froude number), and horizontal mountain aspect ratio (b/a), four classes of wave and flow phenomena of importance in three-dimensional, stratified, uniform, hydrostatic flow past an isolated mountain can be identified (Fig. 5.22):

- (1) linear mountain waves
- (2) wave breaking
- (3) flow splitting
- (4) lee vortices.

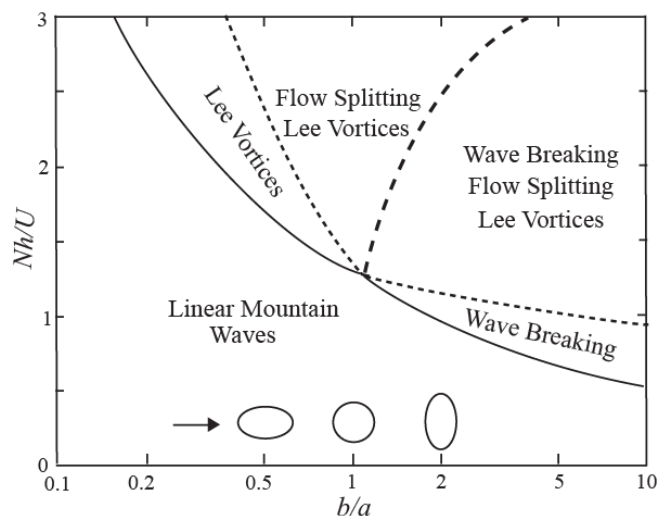


Fig. 5.22: Regime diagram for three-dimensional, stratified, uniform, hydrostatic flow over an isolated mountain. The flow regime is controlled by the horizontal mountain aspect ratio (b/a) and the nondimensional height or the inverse Froude number (Nh/U), where a and b are the mountain scales in along (x) and perpendicular (y) to the basic flow directions, respectively. Four classes of phenomena of importance in this type of flow are: (1) linear mountain waves, (2)

wave breaking, (3) flow splitting, and (4) lee vortices. The circles/ellipses represent the mountain contours. (Lin 2007; Adapted after Smith 1989a and Epifanio 2003)

➤ The key question of the numerically simulated lee vortices as shown in Fig. 5.21 is the source of vorticity.

In the absence of surface friction, boundary layer separation will not occur and thus cannot be held responsible for the formation of the lee vortices.

Although many detailed dynamics of this problem are still topics of current research, the basic dynamics for the generation of lee vortices can be understood through the following two major theories:

- (1) *Tilting of baroclinically-generated vorticity* (Smolarkiewicz and Rotunno 1989) and
- (2) *Generation of internal potential vorticity* by turbulence dissipation in numerical simulations (Smith 1989b; Schär and Smith 1993a, b).

➤ (1) *Tilting of baroclinically-generated vorticity*

The mechanism of baroclinically-generated vorticity tilting can be understood by taking cross differentiations of (2.2.1) – (2.2.3) to yield the inviscid vorticity equation

$$\frac{\partial \boldsymbol{\omega}}{\partial t} = -\mathbf{V} \cdot \nabla \boldsymbol{\omega} + (\boldsymbol{\omega} \cdot \nabla) \mathbf{V} + \frac{\nabla \rho \times \nabla p}{\rho^2}, \quad (5.4.28)$$

where $\boldsymbol{\omega} = \nabla \times \mathbf{V} = (\xi, \eta, \zeta)$ is the *three-dimensional vorticity vector*. The last term on the right side of the above equation represents the generation of vorticity by baroclinicity.

Once local vorticity anomalies are generated, they are advected by the flow field through the first term or tilted and stretched through the second term on the right side of (5.4.28).

For mountains with small aspect ratio of the obstacle height and horizontal width, the baroclinicity term reduces to (e.g., Epifanio 2003):

$$\frac{\nabla \rho \times \nabla p}{\rho^2} \approx -k \times \nabla b, \quad (5.4.29)$$

where b is the buoyancy.

Figure 5.23 shows a schematic diagram depicting the generation of leeside vorticity by the vertical tilting of baroclinically generated horizontal vorticity.

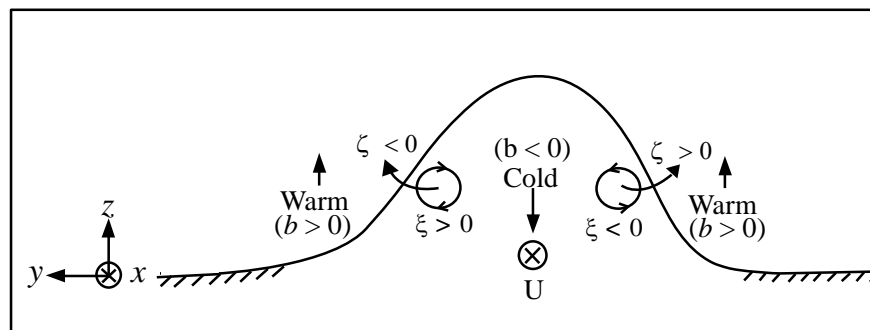


Fig. 5.23: A schematic diagram (Lin 2007) showing the generation of leeside vorticity by the vertical tilting of baroclinically generated horizontal vorticity (Smolarkiewicz and Rotunno

1989). The downward (upward) arrow below the adiabatically-induced cold (warm) region denotes downward (upward) motion. A negative x -vorticity, $\xi < 0$, is produced over the right side of the upslope baroclinically by the relatively cold air ($b < 0$) along the center line and the relatively warm air to the right (facing downstream), as indicated by (5.4.29). This negative x -vorticity is then swept downstream and produces a positive vertical vorticity, $\zeta > 0$, on the right side of the lee due to the vertical tilting of the x -vorticity, as implied by (5.4.28).

A negative x -vorticity, $\xi < 0$, is generated on the right upslope baroclinically by the relatively cold air along the center line and the relatively warm air to the right (facing downstream), as indicated by (5.4.29).

This negative x -vorticity is then swept downstream and produces a positive vertical vorticity, $\zeta > 0$, to the lee by the vertical tilting of the x -vorticity, as implied by (5.4.28).

Similarly, a positive x -vorticity anomaly generated over the left upslope is tilted into a negative vertical vorticity to the lee. As these vertical vorticity anomalies intensify, recirculating warm-core eddies develop as a result of reconnection.

This mechanism dominates during the rapid start-up, early stage, over a nondimensional time $Ut/a = O(1)$, in which the flow is essentially inviscid and adiabatic and the potential vorticity (PV) is conserved (Schär and Durran 1997).

➤ ***(2) Generation of potential vorticity by turbulence dissipation***

- At a later stage, the associated thermal anomalies generated by *baroclinicity* are eroded by dissipative and diffusive processes, whereby the warm surface anomalies are converted into PV.
- During this stage, the flow is controlled by dissipation and is accompanied by the PV generation over a nondimensional time of $O(10) - O(100)$ (Schär and Durran 1997).

Note that the *conservation of potential vorticity* is violated in regions of *flow stagnation*, such as in the region of *upstream blocking* where the isentropic surface intersects the ground, and the *region of wave breaking* above the lee slope where turbulence occurs (Fig. 5.24a).

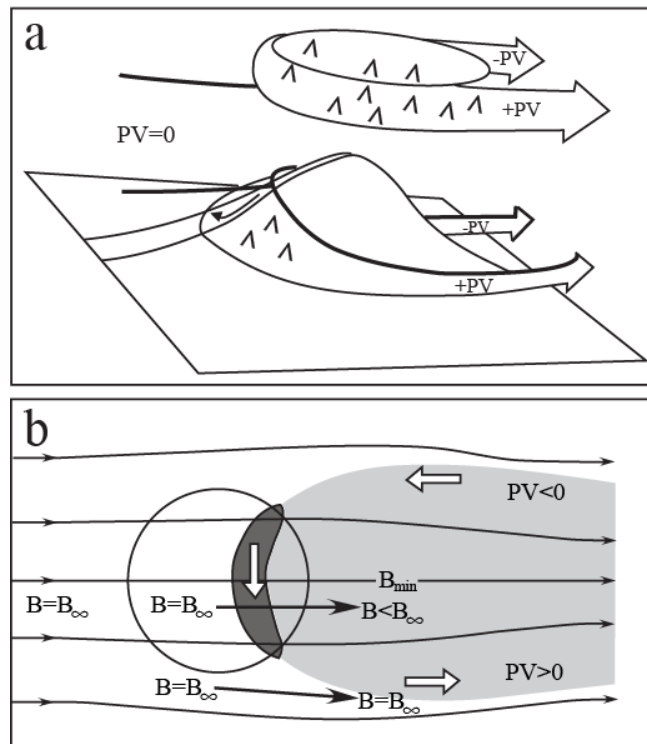


Fig. 5.24: (a) A conceptual model depicting potential vorticity (PV) generation by turbulence dissipation at stagnation points associated with wave breaking aloft and upstream blocking. The symbol “^^^” denotes areas of turbulence generated by wave breaking or blocking. (Adapted after Smith 1989a); (b) Schematic depiction of the relationship between PV generation and Bernoulli function on an isentropic surface in steady-state, stratified flow over the wave breaking region. Thin lines are streamlines and dark-shaded area over the lee slope denotes a localized region of dissipation due to wave breaking, a hydraulic jump or blocking. The grey shaded area extending downstream denotes a reduced Bernoulli function. Open arrows denote the PV flux \mathbf{J} associated with the Bernoulli gradient on the isentropic surface as described by (5.4.35). (Lin 2007; (a) adapted from Smith 1989a and (b) from Schär and Durran 1997)

- The dynamics of dissipative generation of PV is directly linked to the reduction in the Bernoulli function within the wake, as demonstrated in steady shallow-water flow past an obstacle (Schär and Smith 1993a).

The shallow-water theory can be extended to stratified fluid flow by considering the PV (q) which satisfies a conservative equation of the form (Haynes and McIntyre 1990):

$$\frac{\partial(\rho q)}{\partial t} + \nabla \cdot \mathbf{J} = 0, \quad (5.4.30)$$

where q is defined as

$$q = \frac{\nabla \theta \cdot \boldsymbol{\omega}_a}{\rho}, \quad (5.4.31)$$

and the total PV flux (\mathbf{J}) is given by

$$\mathbf{J} = \rho q \mathbf{V} - \left(\dot{Q} \boldsymbol{\omega}_a + \mathbf{F} \times \nabla \theta \right). \quad (5.4.32)$$

In the above equation, \dot{Q} ($\equiv D\theta/Dt$) is the diabatic heating, $\boldsymbol{\omega}_a$ the three-dimensional absolute vorticity vector, and \mathbf{F} the viscous force per unit mass. In this section, we have assumed that the Earth rotation is negligible thus $\boldsymbol{\omega}_a = \boldsymbol{\omega}$.

It can be shown that

$$\mathbf{J} = \nabla\theta \times \left(\nabla B + \frac{\partial \mathbf{V}}{\partial t} \right) - \boldsymbol{\omega} \frac{\partial \theta}{\partial t}, \quad (5.4.33)$$

where

$$B = \mathbf{V} \cdot \mathbf{V} / 2 + c_p T + gz \quad (5.4.34)$$

is the *Bernoulli function*. In a steady state flow, the Bernoulli function is conserved following the flow. In addition, (5.4.33) reduces to

$$\mathbf{J} = \nabla\theta \times \nabla B = \frac{\partial \theta}{\partial \mathbf{n}} \mathbf{n} \times \nabla B, \quad (5.4.35)$$

where \mathbf{n} is a unit vector oriented perpendicular to the isentropic surface and pointing toward warm air.

The *generalized Bernoulli's theorem* (Schär 1993), (5.4.35), indicates that non-zero PV fluxes must be present where there is a variation in the Bernoulli function along any isentropic surface.

Figure 5.24b shows a schematic of PV generation by turbulence dissipation on an isentropic surface in steady-state stratified flow past an isolated mountain.

The narrow dissipative region may be produced by turbulence associated with wave breaking, a hydraulic jump or blocking, and generates Bernoulli function deficit in the wake extending downstream.

Based on (5.4.34), PV is generated in the dissipative region and advected downstream along the edge of the wake. A pair of counter-rotating vortices may form in the wake if the vertical vorticity associated with the generated PV is sufficiently strong.

It appears that the above PV analysis is able to explain the close relationship between dissipative turbulence and PV generation for a low-Froude number, stratified flow over an isolated mountain. The causality, however, is still unclear due to the steady state assumption.

In addition, an assumption of balance is required in order to infer the structure of the flow from the distribution of PV (Hoskins et al. 1985).

In the near field of the wake, these balance constraints are constantly strongly violated due to the presence of the strong surface temperature gradient over the lee slope, which results from the upstream blocking (Epifanio and Rotunno 2005). Therefore, although the PV generation may have important implications on the downstream evolution of orographic wakes and lee vortices, a fundamental understanding of the wake formation is needed.

- When the *wake flow* in which the lee vortices are embedded becomes unstable, the vortices tend to shed downstream and form a *von Kármán vortex street*.

A von Kármán vortex street is a repeating pattern of alternate and swirling vortices along the center line of the wake flow, and is named after the fluid dynamicist, Theodore von Kármán. This process is also known as *vortex shedding*.

Any noise, impulsive disturbance, or asymmetric forcing in the wake flow can trigger an instability, which gives way to a vortex street or vortex shedding.

It needs to be examined whether a vortex shedding requires unstable flow (see [Bridges 2009](#)). Figure 5.25 shows an example of a von Kármán vortex street formed in the atmosphere to the lee of a mountainous island. The von Kármán vortex street or vortex shedding has also been simulated by many nonlinear numerical models, such as that shown in Fig. 5.28a.



Fig. 5.25: A von Kármán vortex street that formed to the lee of the Guadalupe Island, off the coast of Mexico's Baja Peninsula, revealed by MISR images from June 11, 2000 detected by NASA satellite Terra. (From Visible Earth, NASA)